

---

# DEVELOPMENT OF INTERPRETABLE MACHINE LEARNING MODELS TO DETECT ARRHYTHMIA BASED ON ECG DATA

---

A PREPRINT

**Shourya Verma**  
 Universität Heidelberg  
 shourya.verma@stud.uni-heidelberg.de

May 10, 2022

## ABSTRACT

The analysis of electrocardiogram (ECG) signals can be time consuming as it is performed manually by cardiologists. Therefore, automation through machine learning (ML) classification is being increasingly proposed which would allow ML models to learn the features of a heartbeat and detect abnormalities. The lack of interpretability hinders the application of Deep Learning in healthcare. Through interpretability of these models, we would understand how a machine learning algorithm makes its decisions and what patterns are being followed for classification. This thesis builds Convolutional Neural Network (CNN) and Long Short-Term Memory (LSTM) classifiers based on state-of-the-art models and compares their performance and interpretability to shallow classifiers. Here, both global and local interpretability methods are exploited to understand the interaction between dependent and independent variables across the entire dataset and to examine model decisions in each sample, respectively. Partial Dependence Plots, Shapley Additive Explanations, Permutation Feature Importance, and Gradient Weighted Class Activation Maps (Grad-Cam) are the four interpretability techniques implemented on time-series ML models classifying ECG rhythms. In particular, we exploit Grad-Cam, which is a local interpretability technique and examine whether its interpretability varies between correctly and incorrectly classified ECG beats within each class. Furthermore, the classifiers are evaluated using K-Fold cross-validation and Leave Groups Out techniques, and we use non-parametric statistical testing to examine whether differences are significant. It was found that Grad-CAM was the most effective interpretability technique at explaining predictions of proposed CNN and LSTM models. We concluded that all high performing classifiers looked at the QRS complex of the ECG rhythm when making predictions.

**Keywords** Machine Learning, Interpretability, Arrhythmia, Grad-CAM

## 1 Introduction

The Electrocardiogram (ECG) is a medical test that detects cardiac abnormalities by measuring the electrical signals generated by the heart during contraction. This test is the most accessible and inexpensive tool for diagnosing conditions like arrhythmia. Arrhythmia is a cardiac abnormality related to the rate and rhythm of the heartbeat. Despite being the most frequently used diagnosing tool, the rates of ECGs misdiagnosis are still too high. A study from 2016 showed that approximately one in three patients out of 550,000 had their ECGs misdiagnosed and misinterpreted Wu et al. [2018]. This study provides an insight that ECG misrepresentations may have far reaching health diagnostic ramifications. Hence, interpretable ECG algorithms need to be more accurate and explainable so misdiagnoses can be swiftly caught and removed before affecting a patient.

Traditionally, the analysis of these signals can take time as it is performed by cardiologists. Therefore, automation through Machine Learning (ML) classification is being increasingly proposed which would allow ML models to learn the features of a heartbeat and detect abnormalities. The models however fail to recognize unseen ECG data from new datasets while also facing interpretability and explanation problems. These gaps in interpretability of models occur due

to the 'black-box' nature of ML models which render these techniques untrustworthy by clinicians and in-turn limit their application in patient driven healthcare industry.

This paper investigates these concerns by using and building ML models for ECG classification, and implementing Global and Local Interpretability techniques on the models. These models were trained on the MIT-BIH arrhythmia dataset Moody and Mark [2001], where the ECG data was split into single beats and each beat was classified into one of eight beat classes. The ML model algorithms included naive Bayes' and ensemble methods, support vector machines, deep and recurrent neural networks. The results for all the models are compared using non-parametric statistical hypothesis testing, and issues with different interpretability techniques are addressed.

Since most interpretability libraries do not support time-series data very well due to its abundance of data points per instance, the ECG beats were sliced into 11 segments where different group of segments represented the morphology of the ECG beats. These explanations provide important insight on how a model comes to make its decision. This is done by analyzing individual classes and examining correct and mis-classified beats within classes. Global interpretability methods like Partial Dependency Plots Molnar [2019], Shapley Additive Explanations Lundberg and Lee [2017], and Permutation Feature Importance Altmann et al. [2010] were implemented, and Local interpretability approach of Gradient Weighted Class Activation Maps Selvaraju et al. [2017] was applied on Convolutional Neural Network and Long Short-Term Memory Network.

The github repository can be found here: [https://github.com/shouryaverma/interpretable\\_ml\\_ecg](https://github.com/shouryaverma/interpretable_ml_ecg). It contains the source code, the results, and the original thesis document.

## 2 Background

### 2.1 ECG Structure and MIT-BIH Dataset

An ECG test consist of collecting data through the electrical activity of the human cardiovascular system from various different angles by placing electrodes at different points on the skin. This non-invasive method of analysing the heartbeat consist of three key features which represent distinct stages of the heartbeat, i.e the P-wave, which reflects the depolarization of the atria; the QRS complex, which shows the depolarization of the ventricles; and the T-wave, which represents the re-polarization of the ventricles. This allows us to detect abnormalities by equating each phase to the normal cardiac cycle. Figure 1 shows the ECG signal representation of a normal beat. These ECG signals are extremely susceptible to high and low frequency noise which usually occur from baseline wander, misplaced electrode contact, motion artifacts, or power line interference Velayudhan and Peter [2016].

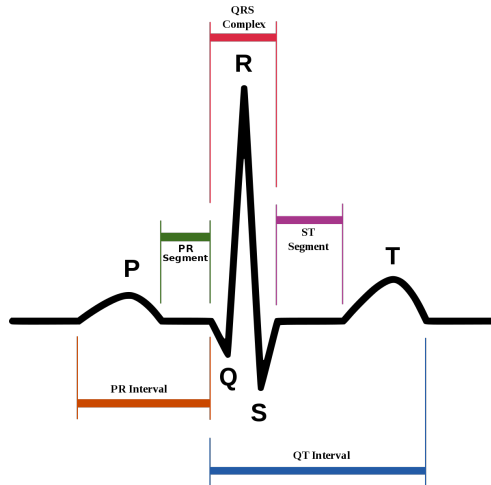


**Figure 1:** Normal ECG Signal

Class	ID	Beat Description
N	1	Normal
L	2	Left Bundle Branch Block
R	3	Right Bundle Branch Block
V	4	Premature Ventricular Contraction
A	5	Atrial Premature
F	6	Fusion of Ventricular and Normal
f	7	Fusion of Paced and Normal
/	8	Paced

**Table 1:** Beat Classes, ID Number, and Description

The MIT-BIH dataset used for this investigation is a public database consisting of a large number of beats, and is frequently used for time-series classification research. The MIT-BIH Arrhythmia Database contains sections of ambulatory ECG recordings, from 47 subjects, digitized at 360 samples per second per channel with 11-bit resolution at 10-mV range on two channels, studied by the BIH Laboratory. Here 23 recordings were picked at random from a set of 4000 24-hour ECG recordings collected from a population 60% of inpatients and 40% outpatients Moody and Mark [2001]. This data has been pre-annotated and labelled by cardiologists. These different annotations refer to various normal and abnormal ECG signals which represent different types of arrhythmia. The dataset consists of ECG signals

of various classes, but the eight classes used for this investigation are 'N', 'L', 'R', 'V', 'A', 'F', 'f', '/'. Table 1 shows the description and numerical identification values assigned to these classes.

## 2.2 Time-series Classification Based on Machine Learning

Machine Learning (ML) has increasingly been used in various areas of research, but despite encouraging results on big-bio datasets, there is still limited number of applications of these algorithms in the healthcare industry. One of the few challenges of ML in healthcare environments is that there is a large discrepancy of consistency in data characteristics as the global population of patients is diverse and expanding, allowing the data to widely vary between different groups of medical patients Kelly et al. [2019]. This makes the data extremely imbalanced due to the presence of rare conditions within sick patients and a more likely chance for a person to be healthy and asymptomatic. This paper implemented supervised machine learning technique called multi-class classification where the goal is to correctly identify the class an input corresponds to. A regular, but awkward solution to time-series classification is to consider every time point as a unique feature and directly apply a standard learning algorithm. In this procedure, the algorithm disregards information accommodated in the time order of the data. If the feature order were shuffled, the predictions would not differ. It is also usual to use deep and recurrent learning to classify time-series. Long Short-Term Memory and Convolutional Neural Networks are deemed capable of extracting dynamical characteristics of time-series, hence their success.

## 2.3 Machine Learning for ECG Classification

This section briefly reviews state-of-the-art research and literature on ECG classification using deep and recurrent neural networks which also include different data resampling techniques and various model architecture. It provides the justification and the overall motivation of creating proposed neural network architectures and using other shallow algorithms as comparison for classification and interpretability.

Kachuee et al. [2018] and Acharya et al. [2017], both proposed deep learning convolutional neural network (CNN) based classification of ECG signals to improve on conventional ML techniques for analysis of ECG like boosted decision trees, support vector machines and neural network multi-layer perceptrons. Both papers used the MIT-BIH arrhythmia dataset and their models displayed an accuracy of 93.40% and 94.90% on noise free ECG classification, respectively. Both papers however only trained and evaluated results on five annotation classes. Despite having 2 less layers than Kachuee et al. [2018], and having a smaller kernel size, Acharya et al. [2017] reported 1.5% better accuracy, likely due to the leaky ReLU activation function (as opposed to normal ReLU) and additional fully connected layer. Pandey and Janghel [2019] proposed an 11-layer CNN to classify five classes of beats in the MIT-BIH arrhythmia dataset, using Synthetic Minority Oversampling Technique (SMOTE) to handle the dataset imbalance. Their network consisted of four 1D-convolution and max pooling layers, followed by two fully connected ReLU layers and a fully connected final softmax layer to classify beats into the five classes. The model was tested using the hold-out method, by randomly splitting their beats into training and testing datasets, achieving an accuracy of 98.3% .

Gao et al. [2019] proposed the use of an LSTM model to classify beats in the MIT-BIH arrhythmia dataset using a focal loss function. They used a 64 filter LSTM layer followed by two fully connected layers to classify beats into one of eight classes and trained their model for 350 epochs. Their model was tested using the hold-out method, with 90% of training data and 10% testing data and achieved an accuracy of 99.30%. Mousavi and Afghah [2019] improved on this work by adding a CNN layer to an LSTM model with sequence-to-sequence networks which consist of recurrent neural network encoder and decoder. SMOTE was used by this paper as well to address issues with imbalanced ECG data in the MIT-BIH dataset. Their model consisted of three 1D-convolutional layers with stride 1, kernel size 2x1, and ReLU activation. Each convolutional layer was followed by a max pooling layer of the same kernel size and stride. The output from these entered a LSTM unit as input, which consisted of the encoder and decoders before creating the output which was done by a softmax layer. This model outperformed the previous work, giving accuracy of 99.92% on noise free, intra-patient, ECG signal paradigm.

Following on from work discussed in this section, this paper describes the creation of a new CNN and LSTM model architecture and classifying 8 annotation classes, along with using models like ensemble algorithms, naive Bayes, support vector machines, and multi-layer perceptrons to compare the proposed deep and recurrent neural networks. The issue of data imbalance is countered by using data resampling techniques during data pre-processing.

## 2.4 Machine Learning Interpretability

The area that investigates the explainable properties of the ML models is called interpretability. It determines if the model are black-boxes or if they have an explainable property. Molnar [2019] defines interpretability as: 'Interpretability is the degree to which a human can consistently predict the model's result'. Stiglic et al. [2019] describes the need for

interpretability of ML models in healthcare. The need for explainable 'black-box' models is important as it will allow the clinicians to make decisions driven by data, which would in turn help patients receive personalized high-quality care. It will improve efficiency in recognizing specific abnormalities help accelerate and optimize treatment.

Interpretability can be divided into having four attributes namely: global and local interpretability, model-specific and model-agnostic interpretability. Figure 2 shows how different interpretability methods can have these attributes. As explained by Molnar [2019], model-specific interpretability tools are confined and specific to one model and depend completely on the features and rules of that particular model. Model-agnostic tools, however, appear to be more applicable to post-hoc methods which can be used on any ML model by analysing input and output feature weights. Global interpretability explains model decisions depending on conditional interactions of the dependent and independent variables and features of the entire dataset, while local interpretability seems to recognize prediction decisions for a single value in the data i.e., for the local region that the point is located at.

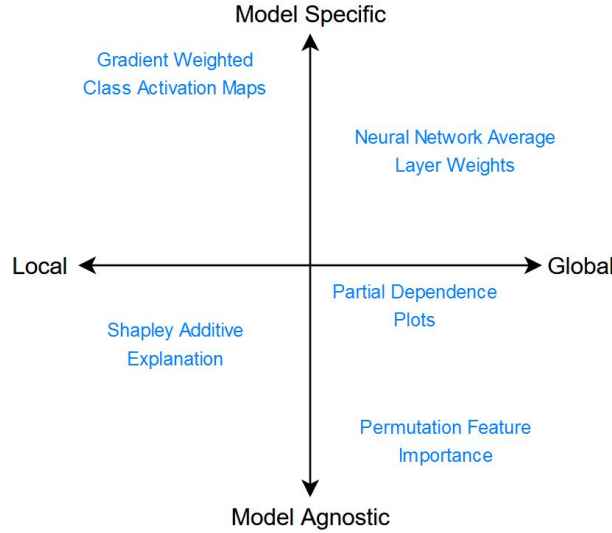


**Figure 2:** A Guide to Interpretability

Vijayarangan et al. [2020] proposed a novel local interpretability technique of using Gradient-weighted Class Activation Map (Grad-CAM) to visualize the saliency on both LSTM and CNN models for ECG data. These saliency visualizations allowed the user to gain insight of the predictions performed by the model. These interpretations, however, were performed on individual time-series using beat-by-beat approach, which was unable to interpret and understand the overall rules of the model's decision on the entire dataset.

Jones et al. [2020] improved this ECG classification technique by applying saliency maps for local interpretability on multiple ECGs of the same class to obtain an average explanation. This allowed for a more general interpretation of the decisions made by the model, capturing all the overarching rules. Their work involved segmentation of saliency maps into blocks for each beat which allowed for quantitative comparison of decision-making process of the model. This was implemented using the keras-vis library which has since been deprecated.

### 3 Methodology

#### 3.1 Data Pre-processing

For reading the MIT-BIH dataset, the native python waveform-database (WFDB) package was used, which is a library of tools for reading, writing, and processing WFDB signals and annotations. This allowed us to obtain all the annotations for all normal and abnormal ECGs.

Referring back to table 1, the annotation classes 'N', 'L', 'R', 'V', 'A', 'F', 'f', '/' were used as most of the ECG signals were assigned to these classes. There is an imbalance in the ECG dataset, where we see an abundance of 'N' beats, while all the other beat classes do not even pass the 10,000 threshold. This also only shows data from one of two channels of the MIT-BIH database. In order to obtain all the beats, ECG signals from both the channels were extracted and stacked. After extracting the 8 important classes that we will be working with and removing all the other classes,

we applied data clean-up processes. The first step was assigning each of the 8 classes a number which would allow us to make the data purely numerical and easy to work with. These assigned numerical values can be seen in table 1.

Secondly, each patient record included a complete set of heartbeats, so each individual beat was extracted from all the records by matching the R-peaks of the ECG with their respective annotation class and appending the class' numerical value at the end of the beat. To make every beat contain equal amount of data points, the R-peaks were centered and equal amount of data points were selected on both sides of the peak, this allowed us to maintain consistency for each beat. To avoid irregular amplitudes between signals, all the beats were standardized. The patient record number was also appended at the end of the beat along with the annotation class number. All the cleaned-up data was stored into one .csv file containing all beats of all records. The beat and patient hold-out methods were used for training and testing, split into 75-25%, and 90-10% respectively.

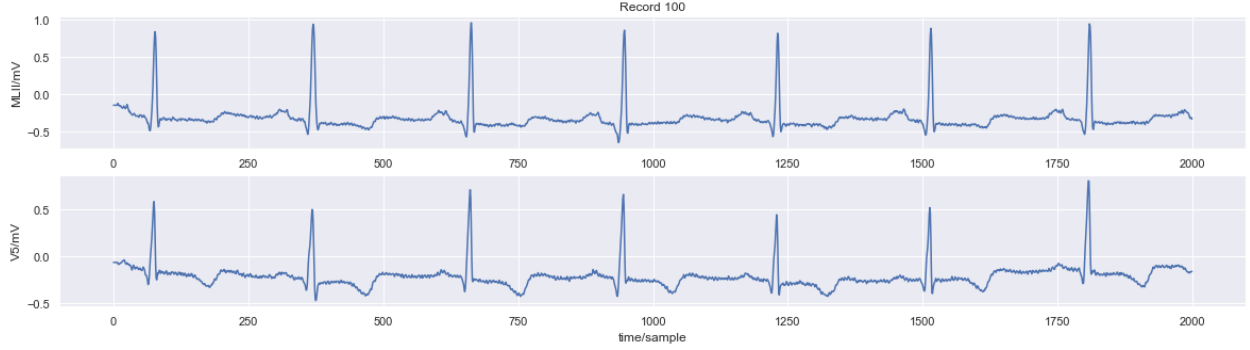


**Figure 3:** Example of Continuous ECG Beats in a Record. (X-Axis: Timestamps, Y-Axis: Voltage)

Figure 3 shows an example of what the original data from MIT-BIH database looked like for one patient in two channels, and as observed, the ECG signals are continuous and not standardized between the two channels and are sampled at 360 Hz. However, figure 4 shows examples of extracted ECG signals with the annotation classes after data pre-processing, allowing us to see the standardization, and r-peak centering implemented on the data points.

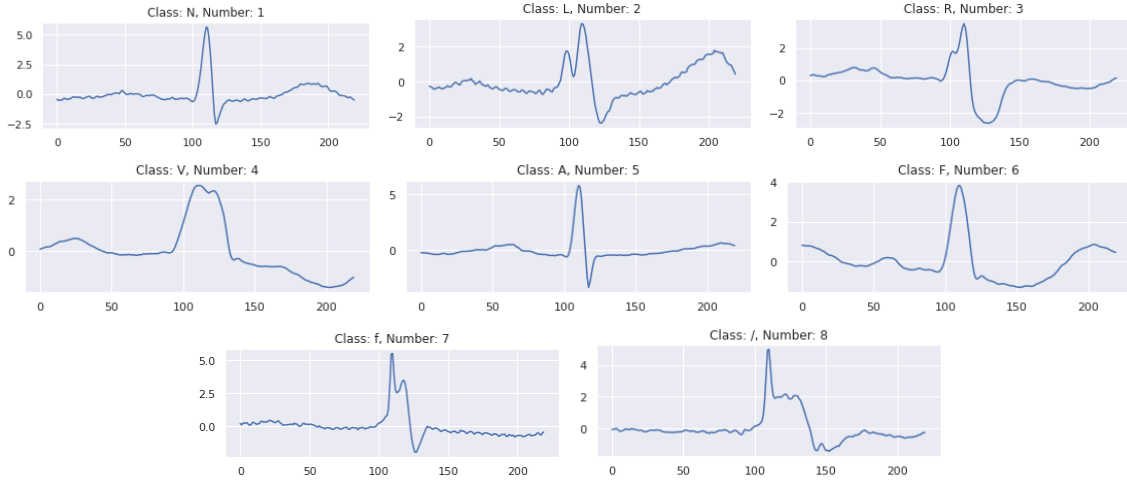


**Figure 4:** Examples of Single Beats of All Classes. (X-Axis: Timestamps, Y-Axis: Voltage)

### 3.2 Data Resampling and Visualization

To address the imbalance between the classes in the MIT-BIH dataset, we used the resample technique by Sci-kit Learn Pedregosa et al. [2011]. This resampling method uses bootstrap method which estimates statistics on a data population by sampling a dataset with replacement through iteration, using a sample size and the number of repeats. For up-sampling and down-sampling, the  $n_{\text{samples}}$  value was calculated by taking the mean values of the total number of beats of the abnormal classes. Figures 5 and 6 show beats with their respective annotation classes from both ECG

channels for beat and patient holdout splits. We observe that after resampling, all the 8 classes in the train dataset have 3989 samples for the beat holdout method and 25789 samples for the patient holdout method.

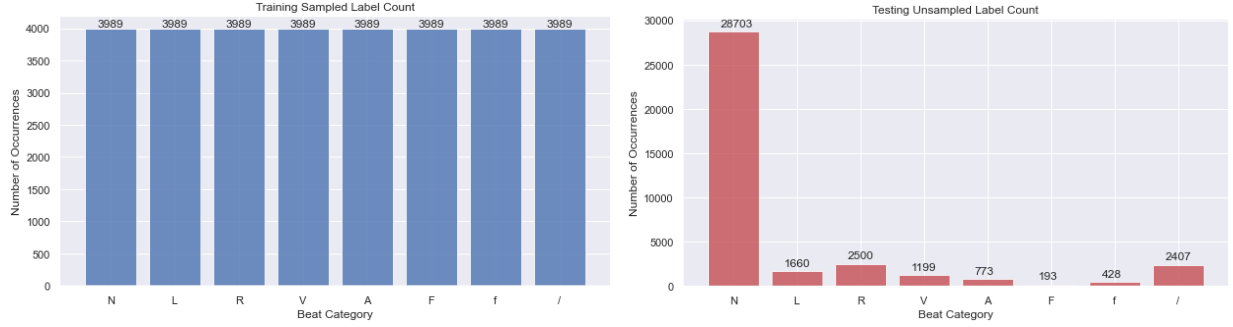


Figure 5: Sampled Train and Test Dataset for Beat Holdout 75/25

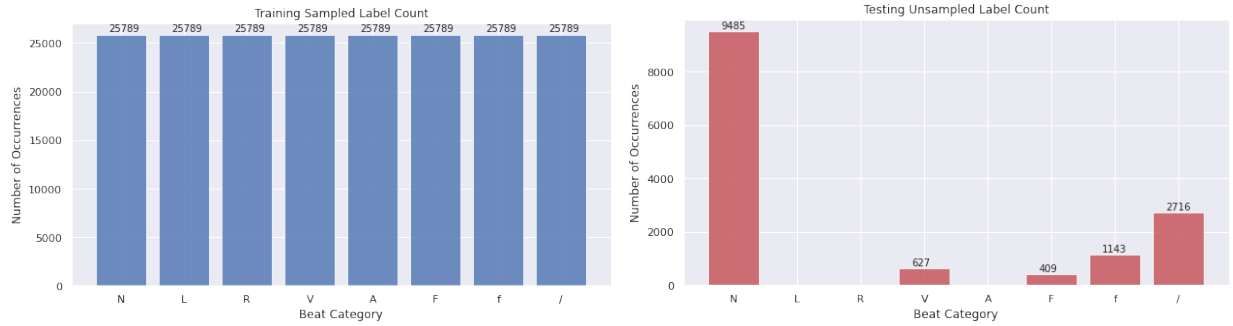


Figure 6: Sampled Train and Test Dataset for Patient Holdout 75/25

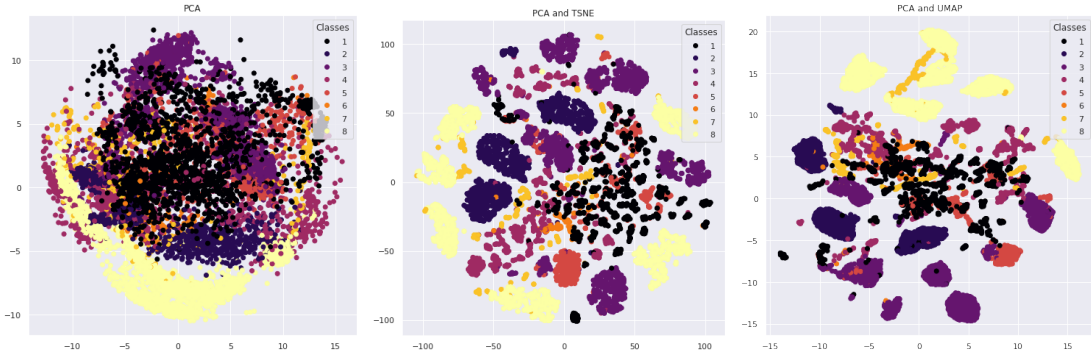


Figure 7: Clustering Unsampled Data per Class

Dimensionality reduction and data visualization techniques were implemented to visualize the ECG classes, since clustering using unsupervised learning is helpful at visualizing different classes and shows us how similar or different the classes behave for unsampled and sampled datasets. These visualization techniques were performed on both unsampled 7 and sampled 8 datasets to understand how close the bootstrap resampling data is clustered to the unsampled data clusters.

Principal Component Analysis (PCA) Jolliffe [2011] was performed on both datasets for dimensionality reduction with  $n\_components$  50. We see in figures, a cloud of data points of different classes but clear clusters were not visible. To improve upon PCA, t-distributed Stochastic Neighbor Embedding (t-SNE) Van der Maaten and Hinton [2008] with  $n\_components$  set to 2 was implemented on PCA. As observed in the sampled figure, it shows us big clusters of different classes, but the data was still fairly spread out. However, for TSNE good clustering was noticed for classes L, R, A and /. To try to further improve this, Uniform Manifold Approximation and Projection (UMAP) McInnes et al. [2018] was implemented on PCA, with  $n\_components$  2 and  $n\_neighbors$  80. As seen in the UMAP figure,

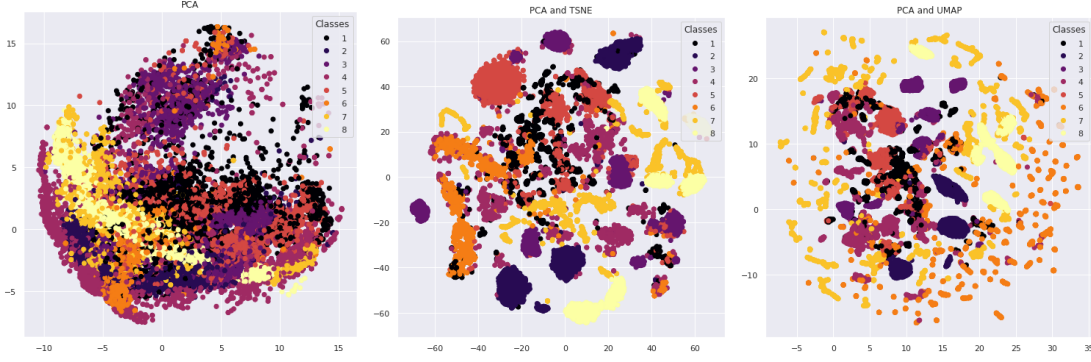


Figure 8: Clustering Sampled Data per Class

the bigger clusters disappear and the data lumps into a balls of smaller clusters which is not very useful in visualizing different classes, but for the unsampled figure, good clustering was noticed for classes N, F, f. These small data lumps can be due to the upsampled beats created by bootstrap resampling techniques which have similar time-series data points.

### 3.3 Machine Learning Models

This paper uses various ML models, specifically Gradient Boosting (GBC), ADA Boosting (ADA), Random Forest (RFC), Gaussian Naive Bayes (NB), Neural Network Multi-Layer Perceptron (NNMLP), C-Support Vector (SVC), Convolutional Neural Network (CNN), and Long Short- Term Memory Network (LSTM). These eight ML classifier models range from ensemble-based algorithms, Bayes algorithm, support vector machine, to deep and recurrent neural networks. This diversified selection of models allows us to investigate and evaluate their performance on multi-class classification of uni-variate time-series ECG data and interpret the best performing models.

#### 3.3.1 Model Architectures and Hyper-parameters

Table 2: Layers of CNN Model

Layer	Filters	Size	Activation
1D-Conv	128	16	ReLU
BatchNorm	—	—	—
1D-Conv	32	16	ReLU
BatchNorm	—	—	—
1D-Conv	9	16	ReLU
1D-MaxPool	—	2	—
Flatten	—	—	—
Dense	512	—	ReLU
Dense	128	—	ReLU
Dense	32	—	ReLU
Dense	9	—	Softmax

Table 3: Layers of LSTM Model

Layer	Filters	Size	Activation
LSTM	128	1	—
LSTM	9	—	—
1D-MaxPool	—	2	—
Flatten	—	—	—
Dense	512	—	ReLU
Dense	128	—	ReLU
Dense	32	—	ReLU
Dense	9	—	Softmax

The CNN model architecture proposed and investigated in this paper is a 11 weighted layer classifier. As seen in table 2, the first four layers of my sequential model are a combination of two 1D-convolutional layers and two batch normalization layer pairs, with kernel size 16, filters 128,32, and activation ReLU for the convolutional layer. The next two layers are the final 1D-convolutional layer with filters 9 and 1D-max pooling layer with pool size 2. The output of the max pooling layer is flattened by a flatten layer and the data is then used as input for the final four fully connected dense layers, where the first three are ReLU activated, and the final layer uses softmax activation for the final output. The model is compiled using the adaptive moment estimation (Adam) optimizer, with the default learning rate of 0.001, and categorical cross-entropy loss function. The model was fit on the training dataset for 10 epochs and 64 batch size.

The LSTM classifier model proposed and investigated in this paper consisted of 8 weighted layers. As seen in table 3, the first two layers were LSTM layers with filter 128 and 9, followed by 1D-max pooling layer with pool size 2. Like the CNN, the max pooling layer's output is flattened by a flatten layer and then is inputted into four fully connected

dense layers with activation ReLU for the first three and softmax for the final layer. The model is compiled using the Adam optimizer, with the default learning rate of 0.001, and categorical cross-entropy loss function. The model was fit on the training dataset for 10 epochs and 256 batch size.

The hyper-parameter for the rest of the models were as follows: both GBC and ADA used  $n\_estimators = 100$ , RFC had  $n\_estimator = 10$  with  $max\_depth = 10$ , NNMLP had  $max\_iter = 100$ , and NB and SVC used their default parameters.

### 3.4 Interpretability Techniques

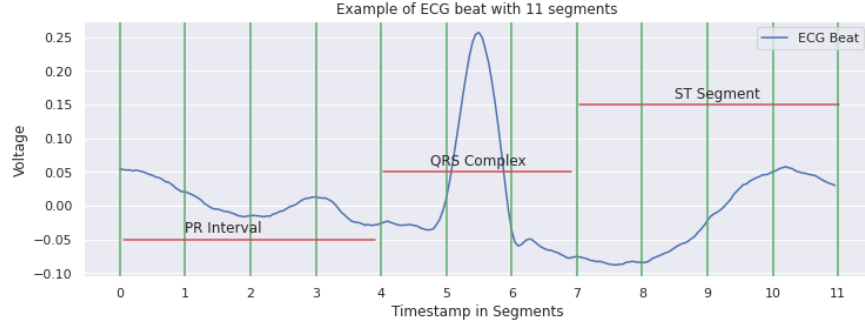


**Figure 9:** ECG Beat Sliced into 11 Segments. (X-Axis: Timestamps, Y-Axis: Voltage)

Once we have the models, we need a way to interpret them, so we can compare the behaviour of each. This section discusses how we do this. The ECG beats were divided into slices of 11 segments which would allow us to understand and interpret which segment is being given more importance by the model during classification. The slices were made by replacing the data points with the average point for each slice. Figure 9 shows a sample ECG beat sliced into 11 segments. Here the segments 1-4 cover the PR interval, the next three segments 5-7 cover the QRS complex and the final four segments 8-11 cover the ST segment. This plot is extremely important as the segment numbers and the names of these group of segments will be frequently mentioned in this entire section. We expected to see the model focusing on important morphological features of the ECG beat, such as the PR interval, the QRS complex, and the ST segment. It could also focus on areas we do not expect due to the capacity of these methods to pick up key features and interactions between pixels in an input image.

#### 3.4.1 Partial Dependency Plots (PDP)

In PDP we expected to see the dependence between the target response and a set of input features of interest, marginalizing over the values of other complementary features.

Two-way PDP were plotted per class and one-way PDP per ECG segment for the NNMLP model, where the normal class was compared against different abnormal classes. For global interpretability, the features are considered to be classes and slices of ECG beats for the complete dataset. The two-way class plots showed that N class as no marginal effect on itself when NNMLP makes its decisions, but every other abnormal class seems to be affected differently by the N class. The per class PDP can be inaccurate as, the practical highest number of features in a partial dependence function is two which is not the fault of PDP, but of the 2-dimensional representation and the inability to comprehend more than 3 dimensions. Since classes are not really features, we move on to one-way PDP to explain the NNMLP model per segment.

The one-way plot per segment showed that segments 1 and 5 have a similar dependence curve. This tells us that this pair of 1 and 5 segments have the same marginal effect on NNMLP’s decision-making process. As for other segments, each of them shows a different partial dependence curve which means that their marginal effect on the predicted outcome of NNMLP was unique, but this did not allow us to interpret the model’s predictions. The relevant graphs can be found in the github repository.

This interpretability technique did not allow us to clearly understand the dependence between features for most segments and had no scope to be quantitatively analysed. Since PDP provide an extremely global interpretation, we move on to techniques which would allow us to further investigate interpretability in a deeper aspect.

### 3.4.2 Shapley Additive Explanations (SHAP)

With SHAP we expected a visual explanation of the model by using shapley values to calculate the importance of a feature by comparing what a model predicts with and without the feature. The desired result would be to obtain ECG segments considered important by the SVC model in each class.

KernelSHAP technique was implemented to calculate feature importance for the SVC model as it does not support TensorFlow models on uni-variate time-series data yet. SHAP summary plot was calculated for ECG segments which allowed us to see the behaviour of each segment for every class. SHAP treats the segments of the ECG as features and explains the model's decision by giving it a SHAP value, so the 11 segments of the ECG beats are shown as features 0 through 10.

In figure 10, the summary plots show the mean of the SHAP values i.e the average impact the features and classes had on the magnitude of the model's outcome. Here we see that features 5, 6, 7 were the most important segments overall but the effect of each individual class can be noticed to be different. The figure 11 takes the global aggregate of the SHAP values and displays them on top of a sample ECG beat. We observe that segments 5, 6, 7 are clearly considered more important than the other segments in a global visualization, which represents the QRS complex. Local visualizations were not possible as SHAP explained only a fraction of instances of the test data, which is not enough to give reliable results.

These interpretability techniques explain a lot about the model's decision-making process and gives accurate explanations, but KernelSHAP is extremely time consuming and interprets only the first 50 instances of the data, making it not fit for explaining deep and recurrent neural networks for time-series data. An alternative for the feature importance method used in SHAP is permutation feature importance, which is explored in the next sub-section.

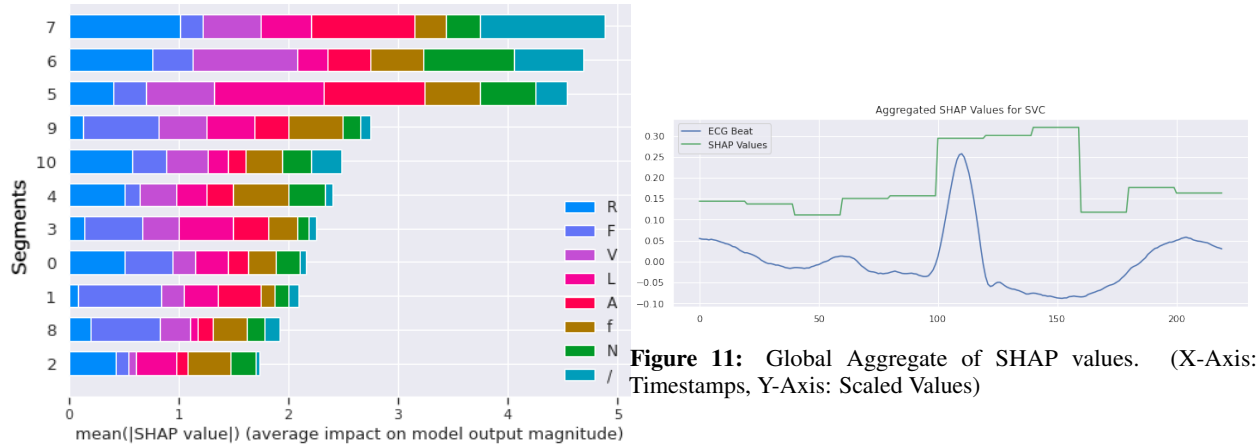


Figure 10: SHAP Summary Plot

### 3.4.3 Permutation Feature Importance (PFI)

In PFI we expected to see importance weights assigned to different ECG segments and which segment each model considers the most important. This technique works for SK-Learn and TensorFlow (using a surrogate model) models which allows us to compare these feature importance scores between each of the classifiers. These values can be quantitatively analysed making PFI easier to evaluate.

The ELI5 library, which allows to explain weights and predictions of a classifier, was used for the computation of PFI. This library provides a way to compute feature importance for any black-box estimator by measuring how score decreases when a feature is unavailable. More figures can be found on github, where the top three segments (features) in most classifiers are 5, 6, 7. which represent the QRS complex in the ECG beats, shown in figure 9. The interpretation is global since we are looking at the complete data as opposed to a single class or a single beat. This interpretation, however global, allows us to consistently explain the predictions of all the models. This method proves to be more helpful as unlike SHAP and PDP methods, it works on all classifiers.

In figure 12, the feature importance scores are represented on a sample ECG beat to better visualize the explanation of this method for each classifier. It can be observed that GBC, RFC, NNMLP, SVC, and CNN give the QRS complex of the ECG beat the highest feature importance. For ADA and NB, these classifiers give lesser importance to the QRS complex but still higher than other segments. The LSTM classifier gives the ST segment higher importance than the

QRS complex. However, these results include all the classes of the classified beats which is a very global interpretation of the explanation of the model’s decision. Since we cannot obtain the PFI per class, the classified beats were separated into correctly and the incorrectly classified beats and implement feature importance on them.



**Figure 12:** Feature Importance of all Models on Sample ECG Beat. (X-Axis: Timestamps, Y-Axis: Scaled Values)

Figure 13 shows the representation of PFI weights per segment for the correctly classified and mis-classified beats for NNMLP and SVC models on a sample ECG beat. We notice that the feature importance representation of the mis-classified beats (in red) does not clearly show important ECG segments. The correct segments (in green) however, show that the QRS complex is given higher importance weights compared to the other segments. We would expect the model to look at the QRS complex, and so the correctly classified beat plot makes sense. The fact that with mis-classified beats the model is looking everywhere, suggests that the model does not know where to look.

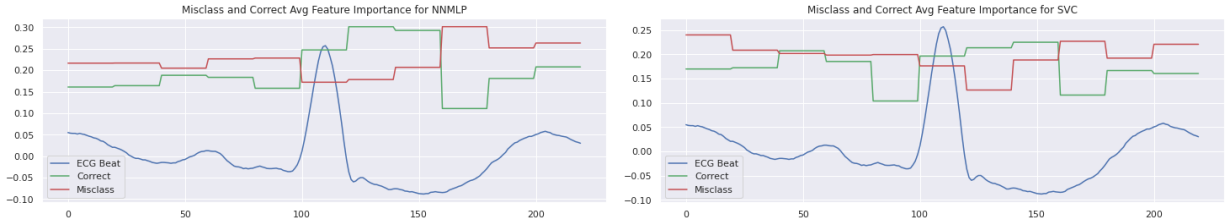


**Figure 13:** Feature Importance of Correctly and Incorrectly Classified Beats on Sample ECG Beat. (X-Axis: Timestamps, Y-Axis: Scaled Values)

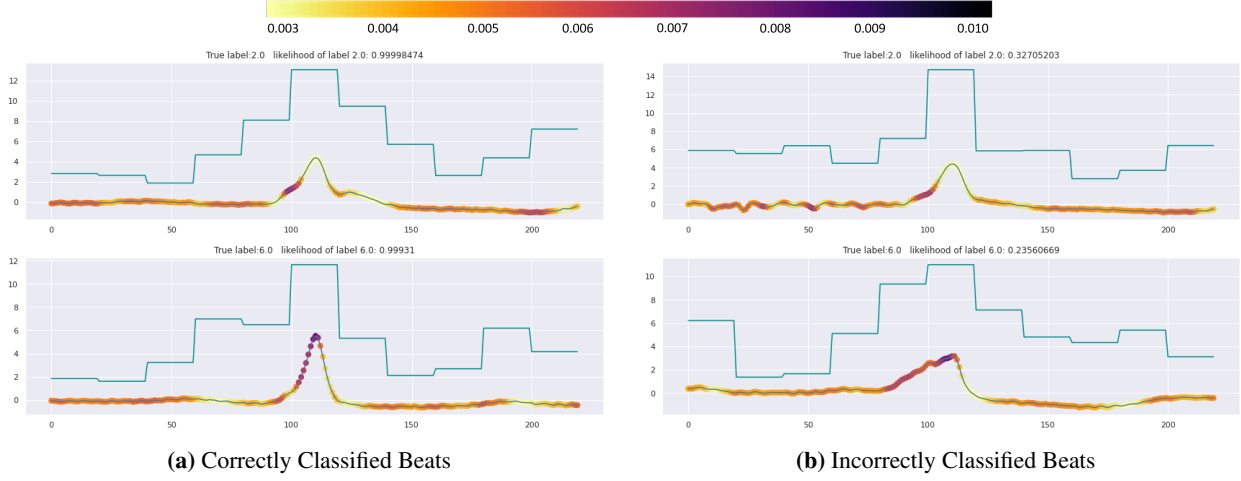
PFI gave us quantitative values of the prediction of the models per segment, this can be considered a global explanation of the model as it focuses on the entire dataset and the drawback of global interpretation techniques is that we cannot look at explanation of specific beats and classes. Grad-CAM will explore a more local interpretation of each beat along with the correct and incorrectly classified beats for the TensorFlow CNN and LSTM models in the next section.

### 3.4.4 Gradient-Weighted Class Activation Maps (Grad-CAM)

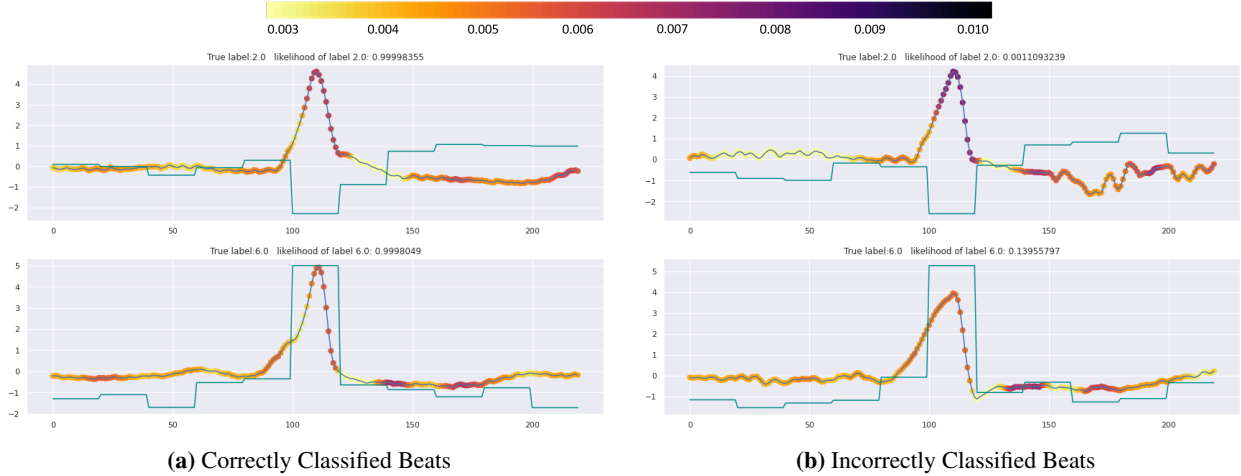
In the Grad-CAM implementation we expected to see a class-specific saliency heat-map of the ECG beats. The higher Grad-CAM values will indicate the data points and segments that the layers of the models give higher gradient weights to, which means that they are more important. The darker and lighter segments of the heat-map will indicate higher and lower Grad-CAM values, respectively.

Grad-CAM for time-series saliency was implemented on the final convolutional layer for the CNN model and the final LSTM layer for the LSTM model. Using the keras back-end function, the weights for these final layers as well as the softmax layer were obtained and the CAM formula 2.4 was implemented on the values. This gave us the activation for the final layers and the obtained values were plotted using a scatter plot on the ECG beats. We visualize in figures 14 and 15 that the discriminating regions of the time-series for the correct and incorrect classes are highlighted. The title indicates the arrhythmia beat class label and the probability values of predicted class. To allow us to visualize which ECG segment is being deemed the most important by the classifiers, the layer weight values were averaged for each

segment and plotted in green. The scale provided on top of the plots indicate the range Grad-CAM values of the final layers.



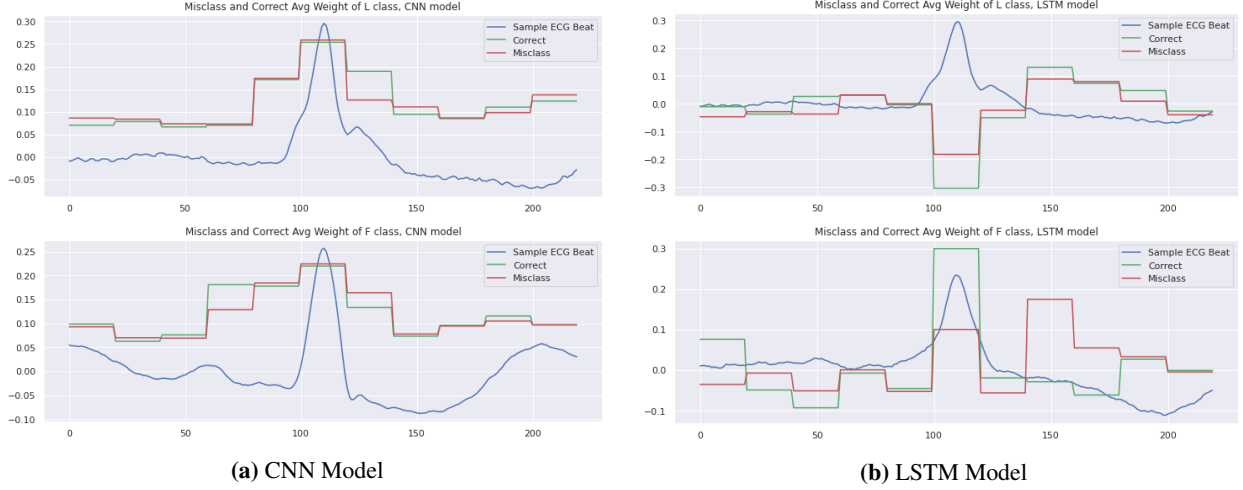
**Figure 14:** Grad-CAM (heat-map) and Layer Weights (in green) per L (top) and F (bottom) Class for CNN. (X-Axis: Timestamps, Y-Axis: Scaled Values)



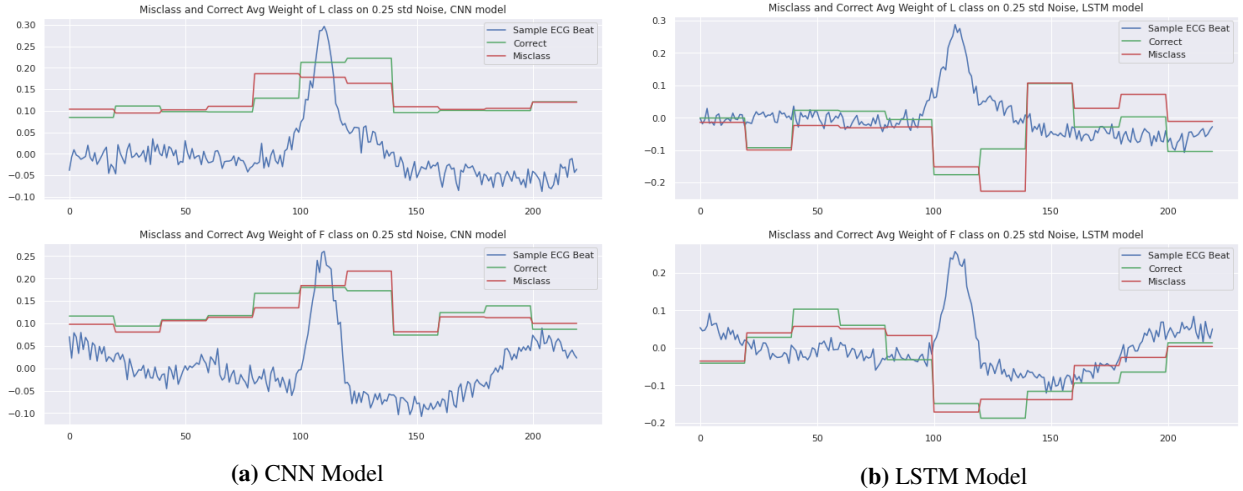
**Figure 15:** Grad-CAM (heat-map) and Layer Weights (in green) per L (top) and F (bottom) Class for LSTM. (X-Axis: Timestamps, Y-Axis: Scaled Values)

Figure 14 and 15 shows the saliency maps for an individual beat of classes L and F for CNN and LSTM models, respectively. We see that in figure 14 the QRS complex is being considered the most important by the CNN model for the classification process. Although in figure 15, it is not clear which segment is deemed as more important by the LSTM model, the Grad-CAM values are discriminating the QRS complex way more than the CNN model, as the R-peaks can be seen having darker scatter points than the PR interval.

More figures on github show the average layer weights of all correctly and incorrectly classified beats for CNN and LSTM model, respectively. The models, on average, are looking at the segments of both correct and incorrectly classified beats equally. This however is a very global interpretation and does not actually tell us about the model's behaviour per class. To visualize a more local interpretation of the models, the average weights for L and F classes are seen in figure 16. Here it is observed that the CNN model is giving higher importance to the QRS complex for both L and F classes, while the LSTM model focuses more on the ST segments while making the classification decisions. This observation is supported by the PFI weights for CNN and LSTM from figure 12. Plots for rest of the classes can be found on github, where we can locally interpret the explanation of both the models' and compare these explanations between all eight classes.



**Figure 16:** Average Layer Weights per L (top) and F (bottom) Class for CNN and LSTM. (X-Axis: Timestamps, Y-Axis: Scaled Values)



**Figure 17:** Average Layer Weights per L (top) and F (bottom) Class for std 0.25 Noise on Test Data for CNN and LSTM. (X-Axis: Timestamps, Y-Axis: Scaled Values)

To examine the robustness of Grad-CAM and layer weight interpretability maps, slightly different test data was used by introducing Gaussian noise and examining the correctly and incorrectly classified samples. The distributions of the noise were created by taking standard deviation of the test data. Low frequency noise, anything less than about 20Hz can be caused by a patient moving when the ECG is being taken and high frequency noise can be caused by a faulty electrode or general electrical noise Kher [2019]. To mimic these scenarios, Gaussian noise of std 0.25 was introduced in the test data. In figure 17 we see that the CNN model is still focusing on the QRS complex in both L and F classes for classification, while the LSTM model seems to be focusing on the ST segment in L class and the PR interval in the F class.

This allows us to conclude that introducing noise in the dataset does not completely weaken the ability of the classifiers in making predictions. Although the important segments are not clearly being distinguished for the LSTM model, the CNN model still focuses on the same segments it was looking at in the data without noise. The robustness of the interpretability is also verified, as the effective segments of the layer weights in figure 17 mostly agree with figure 16, which means that the models dealt with noisy data pretty well. Although their performance may vary on completely new datasets with ECG beats obtained from different patients.

To conclude this subsection, we observed that Grad-CAM was able to interpret the ECG signals locally and globally. This method explained the predictions of both convolutional and recurrent neural networks at each time-series data

point per beat and also allowed us to understand the overall behaviour of the model. The models mostly gravitated towards the QRS complex being the most important segment while making predictions, although it did differ slightly depending on the type of class. Classes L and F were used for Grad-CAM explanation in the main text, and explanation of the rest of the classes can be found on github.

### 3.4.5 Summary

The methodology chapter explained the data pre-processing and visualization techniques, along with mentioning the architectures and hyper-parameters of different models used in this experiment. Since most interpretability libraries do not support time-series data, the ECG beats were sliced into 11 segments where different group of segments represented the morphology of the ECG beat i.e., the PR interval, QRS complex, and the ST segment. The implementation process of the four interpretability techniques used in this investigation was described. These interpretability methods were performed on the first fold of the K-fold cross validation evaluation of the model. PDP turned out to be extremely uninformative at explaining the NNMLP model, while SHAP on SVC was extremely time consuming and explained a fraction of instances of the dataset. PFI being the only model agnostic technique, gave global explanations of all models. Grad-CAM gave both local and global explanations of deep learning CNN and LSTM models.

## 4 Results and Evaluation

The models were running on Google Co-laboratory notebooks utilizing the GPU. After training and fitting the models on the dataset, performance metrics were calculated which included precision-recall, F1-scores, and accuracy for each class and for the complete dataset as well. The documentation Pedregosa et al. [2011] describes precision-recall as: 'In information retrieval, precision is a measure of result relevancy, while recall is a measure of how many truly relevant results are returned.', F1 scores as: 'The F1 score can be interpreted as a weighted average of the precision and recall, where an  $F1$  score reaches its best value at 1 and worst score at 0.' and accuracy as: 'The set of labels predicted for a sample must exactly match the corresponding set of labels in target.'

### 4.1 K-Fold Cross-Validation (Holdout Beats)

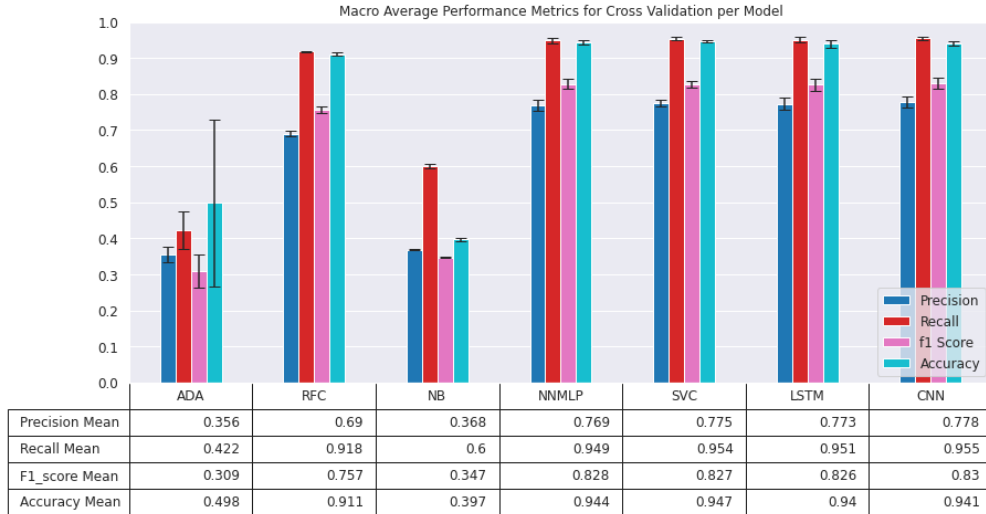


**Figure 18:** Macro Average Performance Metrics per Model on K-fold Cross-Validation. (X-Axis: Models, Y-Axis: Scores)

Cross-validation is used to quantitatively estimate and compare the performance of an ML model on unseen data to estimate the model's general performance. Stratified K-Fold cross-validation was performed on the complete unsampled dataset for all the classifier models with 6 folds, which allowed the given data to be split into 6 different groups for testing and training purposes where the distribution of classes is maintained in the test and train data. The K-Fold cross-validation shuffles the dataset randomly and splits it into k groups, and from each group it obtains a group as hold out while using the rest of it for training.

#### 4.1.1 Classification Performance Metrics

The model is evaluated, and the evaluation score is retained, and the model is reset for the next fold. Each observation in the data is assigned to a specific group and remains in that group for the duration of the procedure, which allows each sample to be used as hold out once and to train k-1 times. The results of the K-Fold cross-validation are summarized with the mean metric score with the standard deviation between the 6 folds, the metrics are mentioned in figure 18. Since gradient boosting classifier in SK-Learn does not support multi-threading, 6 fold cross-validation was taking more than 4 hours to compute, so it was discarded. The macro average score does not consider the proportions of each label in the dataset, while the weighted average performance metrics considers the number of instances of each class while calculating the results, this allows for the metrics to account for imbalance in classes, and results for these can be found on github. Note that interpretability techniques were performed on the models' first cross-validation fold.

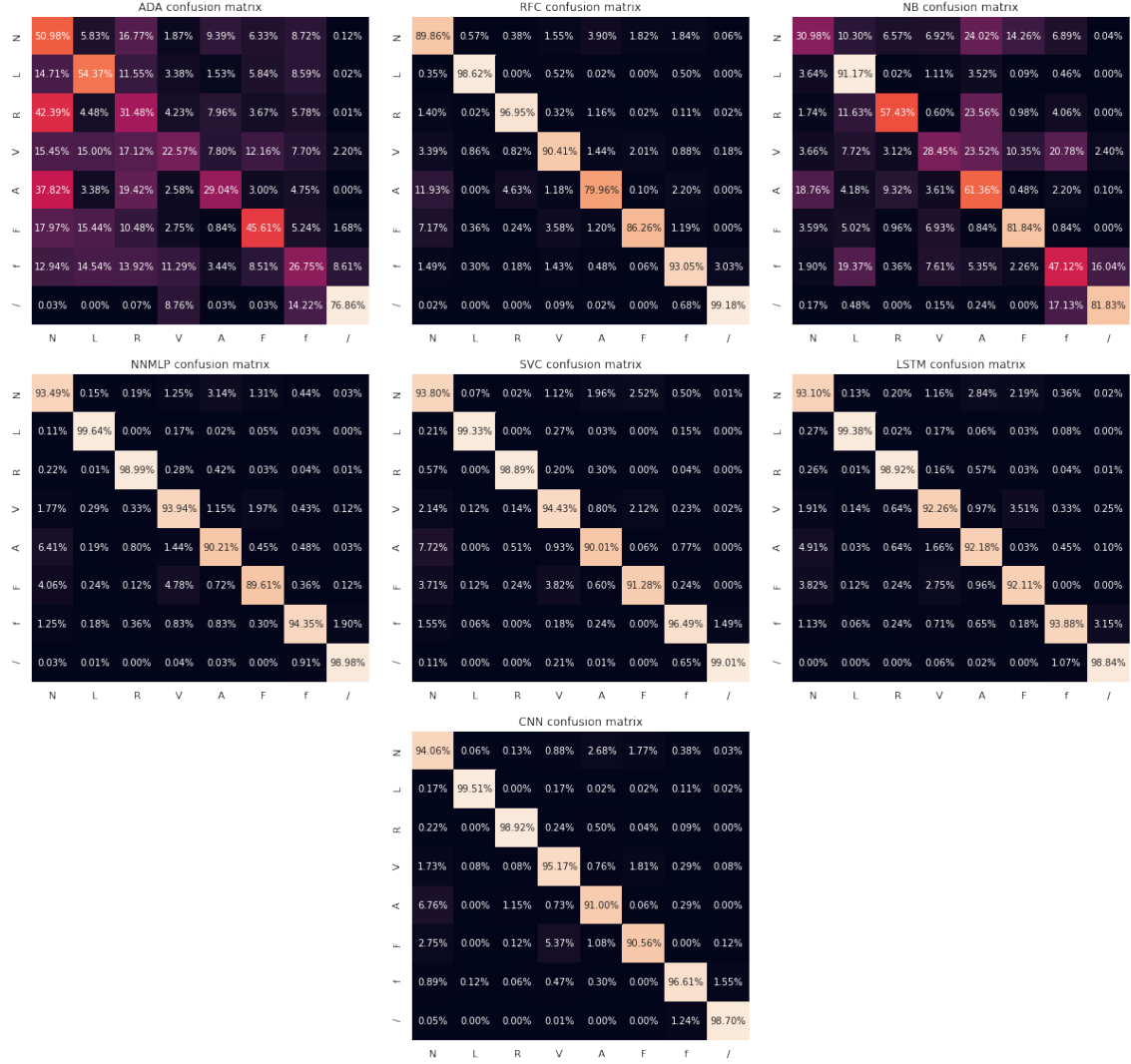


**Figure 19:** Examples of Single Beats of All Classes. (X-Axis: Timestamps, Y-Axis: Voltage) Cross-Validation Confusion Matrices per Model per Class. (X-Axis: Predicted Labels, Y-Axis: True Labels)

To visualize which how many beats were correctly classified into their respective classes and how many were misclassified, confusion matrices were plotted for all the models. The confusion matrix is a symmetric 2-D matrix, where the size of the confusion matrix is the number of classes. The higher the value of the diagonals of a confusion matrix, the higher the performance of the classifier.

We observe in figure 19 that ADA and NB have the most irregular diagonals which explains their bad performance metric values, as this irregularity means the true classes do not correspond to the classified classes. As for the rest of the models, the diagonal is clearly showing 80% and above correct classifications. We observe that for all the classifiers, L

R and / classes are correctly classified with consistently over 90%. We also notice that for N class, ADA and NB have approximately 27% correct classifications, whereas for all other classifiers it is over 80%. NB assumes that all features are independent, which clearly is not the case with a time-dependent ECG, hence giving poor results. As for ADA, it is extremely sensitive to Noisy data and outliers, and also learns progressively. This allows us to consider ADA and NB not fit for ECG beat classification. Analysing this by class, we see that all models give the worst result for classes A and F compared to the rest of the classes. This could be because beats of class A are very similar to class N beats. As for class F, this class has the least number of beats in the dataset and naive bootstrap up-sampling is not enough to make most models learn features accurately. Precision, recall and F1 scores for all models per class can be found [github](#).

#### 4.1.2 Quantitative Analysis

This section will analyse the performance metrics results through statistical tests like Shapiro-Wilk, Kruskal Wallis H, and Wilcoxon signed rank test Carrasco et al. [2020] Demšar [2006]. We will investigate different quantitative analysis methods as well, like Kendall tau rank correlation and also compare PFI and Grad-CAM values. Analysis on the cross-validation performance metrics were implemented to obtain the 95% Confidence Interval (CI). The Shapiro-Wilk test tests the null hypothesis that the data was drawn from a normal distribution. The Kruskal-Wallis H-test tests the null hypothesis that the population mean of all the groups are equal, which is a non-parametric version of one-way Analysis of Variance (ANOVA).



**Figure 20:** All Models Performance Metrics

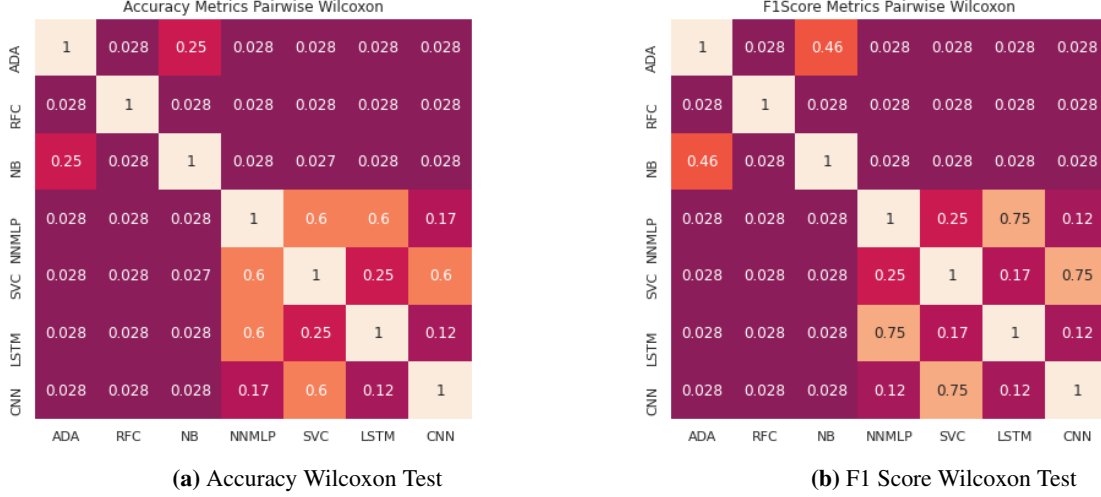
Variable	95% Conf.	Interval	Kruskal Wallis H
Accuracy	0.574	1.019	$1.03e - 5$
Precision	0.463	0.824	$1.09e - 5$
Recall	0.619	1.023	$6.78e - 6$
f1 Score	0.454	0.895	$1.19e - 5$

**Table 4:** Cross-Validation Statistical Analysis

In table 4 the 95% CI shows the probability of a parameter falling between values around the mean. The confidence intervals compute the degree of certainty in a sampling method. CI of accuracy, precision, recall, and f1 score are almost equally spread out which indicates that all of their population means are in similar ranges. Shapiro-Wilk normality test was performed on the metrics where most of the metrics rejected the null hypothesis but not all, hence Kruskal-Wallis H test was performed instead of ANOVA, since non-parametric tests are more robust in this case Virtanen et al. [2020]. The p-values of the Kruskal Wallis H test are exceedingly lower than the significant level of 0.05, which means the null hypothesis is rejected and the population mean of all the groups are not the same.

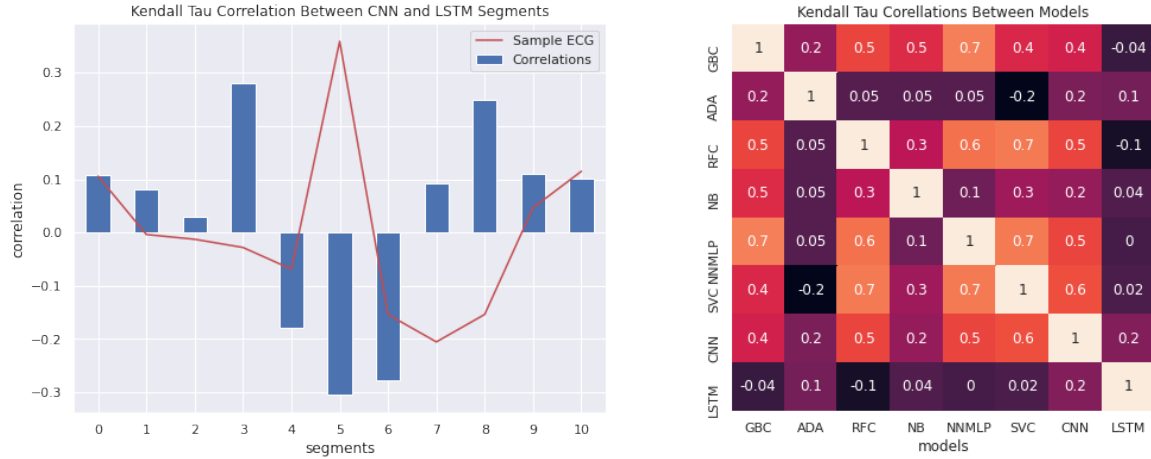
In figure 21, for the Wilcoxon Signed-Rank test, the null hypothesis is rejected when that the results are statistically significant. It is observed that pairwise comparison of NNMLP, SVC, LSTM, and CNN have p-value greater than 0.05 which means that the null hypothesis is rejected and the accuracy and f1 score data have identical population distribution for each cross-validation fold. This means that the results obtained are statistically significant and not obtained by chance.

Figure 22a shows the Kendall’s tau correlation Knight [1966] values per segment between CNN and LSTM layer weights. Here we observe that the values of all the segments except 4, 5, 6 are between 0.0 and 0.3 which show a moderate agreement of correlation between CNN and LSTM weights, whereas segments 4, 5, 6 shows a moderate disagreement of correlation. This disagreement on the QRS complex (as shown over the sample ECG) means that the layer weights of the CNN and LSTM give different importance to the QRS complex and mostly agree on the PR interval and the ST segment. This disagreement on the QRS complex can be visualized in the next figure where the average Grad-CAM values for both CNN and LSTM model are not the same at the segments 4, 5, 6. Figure 22b shows the pairwise Kendall’s tau correlation for the PFI scores between models. Here it can be observed that values closer to 1 show an extremely strong correlation while the values closer to 0 which indicates absence of association through null



**Figure 21:** Pairwise Wilcoxon Signed-Rank Test per Model for Performance Metrics, P-values

hypothesis. PFI values of ADA, NB and LSTM have the almost no correlation with other models. This could be due to the bad performance of ADA and NB models, whereas for the LSTM model, it could be the results of the feature importance scores favouring completely different segments than the other models. This can be better seen in the next figure which visualizes the PFI values for the LSTM model.



(a) Per Segment Correlation between CNN and LSTM Layer Weights (b) Per Model Correlation between Feature Weights

**Figure 22:** Kendall Tau Correlations P-values

We then move on to quantitatively analyse and compare PFI feature importance weights and Grad-CAM correct and mis-classified results per segment. This is done by scaling the results and plotting the mean and 25% - 75% quantile range of Grad-CAM values along with the obtained PFI values. As seen in figure 23 we observe that the average plot for CNN and LSTM focus on the QRS complex and the ST segment, respectively. For the L class plots, PFI and Grad-CAM values agree with each other as they both focus on the same segments. As for F class plots, the values did not quite agree with the important segments. This is because F class is more likely to be mis-classified than the L class, as seen in the confusion matrices results.

## 4.2 Leave Groups Out (Holdout Patients)

After K-fold validation on traditional holdout method which tested on unseen beats, the Leave Groups Out approach was used to evaluate the classifier performance. This method allows us to test on unseen patients as patient number 104, 113, 119, 208, and 210 were split from the dataset to be used for testing, while the remaining 43 patients were used for

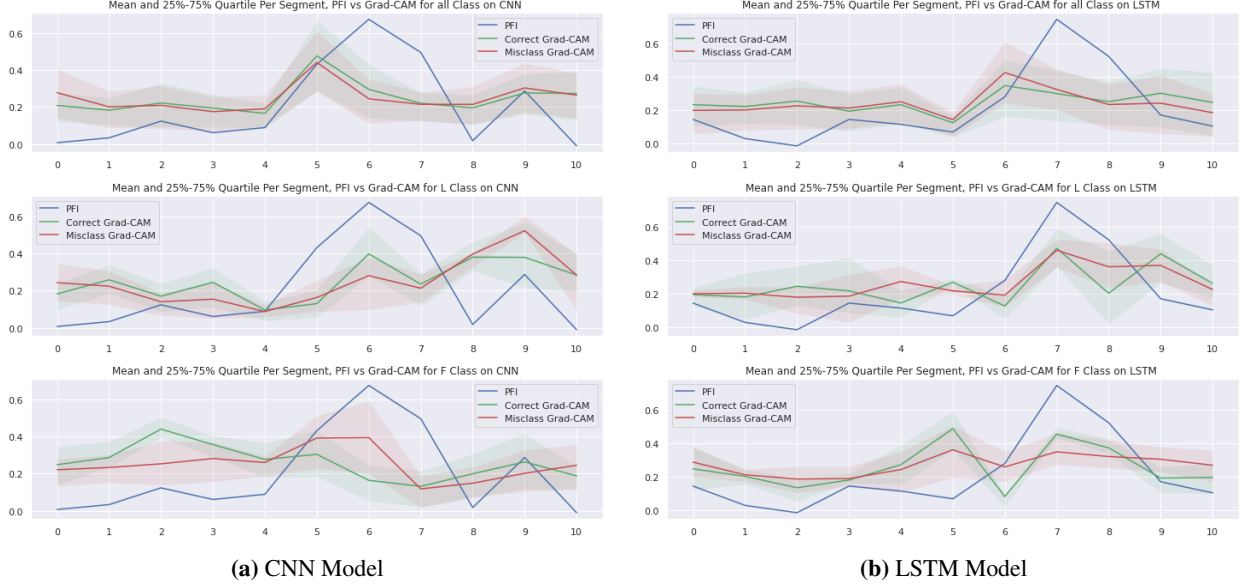


**Figure 23:** Mean and 25%-75% Quartile Values Per Segment - PFI vs Grad-CAM Average (top), L Class (middle), F Class (bottom), for CNN and LSTM Models. (X-Axis: Segments, Y-Axis: Scaled Values)

training. Holding out patients from the dataset instead of beats leads to the risk of also removing classes of ECG beats, since a few abnormalities may be limited to one or two patients. The same method has also been used by Jones et al. [2020], where they also chose the same patient numbers to hold out. The selected patients however do not contain any beats from classes L, R, and A.

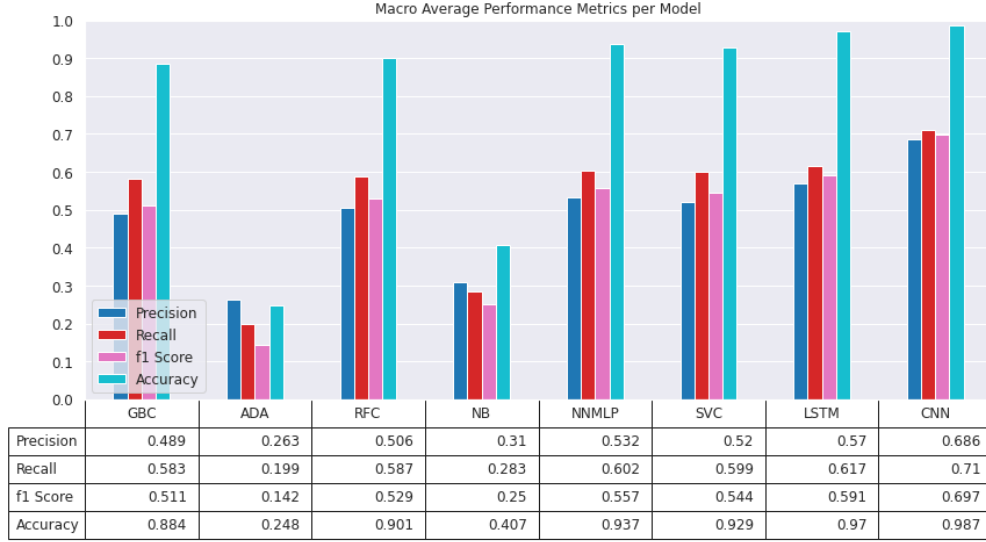


**Figure 24:** Macro Average Leave Groups Out Performance Metrics per Model. (X-Axis: Models, Y-Axis: Scores)

Patient holdout method allowed us to test on beats from unseen patients, whereas the beat holdout method shuffled beats of all patients for training and testing purposes. Although testing using the beat holdout method is considered the most common method, it can result in flawed results due to data leakage. Separating ECG recordings by beats and randomly splitting a shuffled set of these beats for testing results in having beats in both the training and testing dataset from the same patient. Due to similar characteristics of patients like electrode placement, pre-existing conditions, and medications, there is a chance of common morphology between beats. In simpler terms, a beat from one patient will probably look same as another beat (of the same class) from the same patient. This results in data bleeding between the training and dataset, which should be avoided Jones et al. [2020].

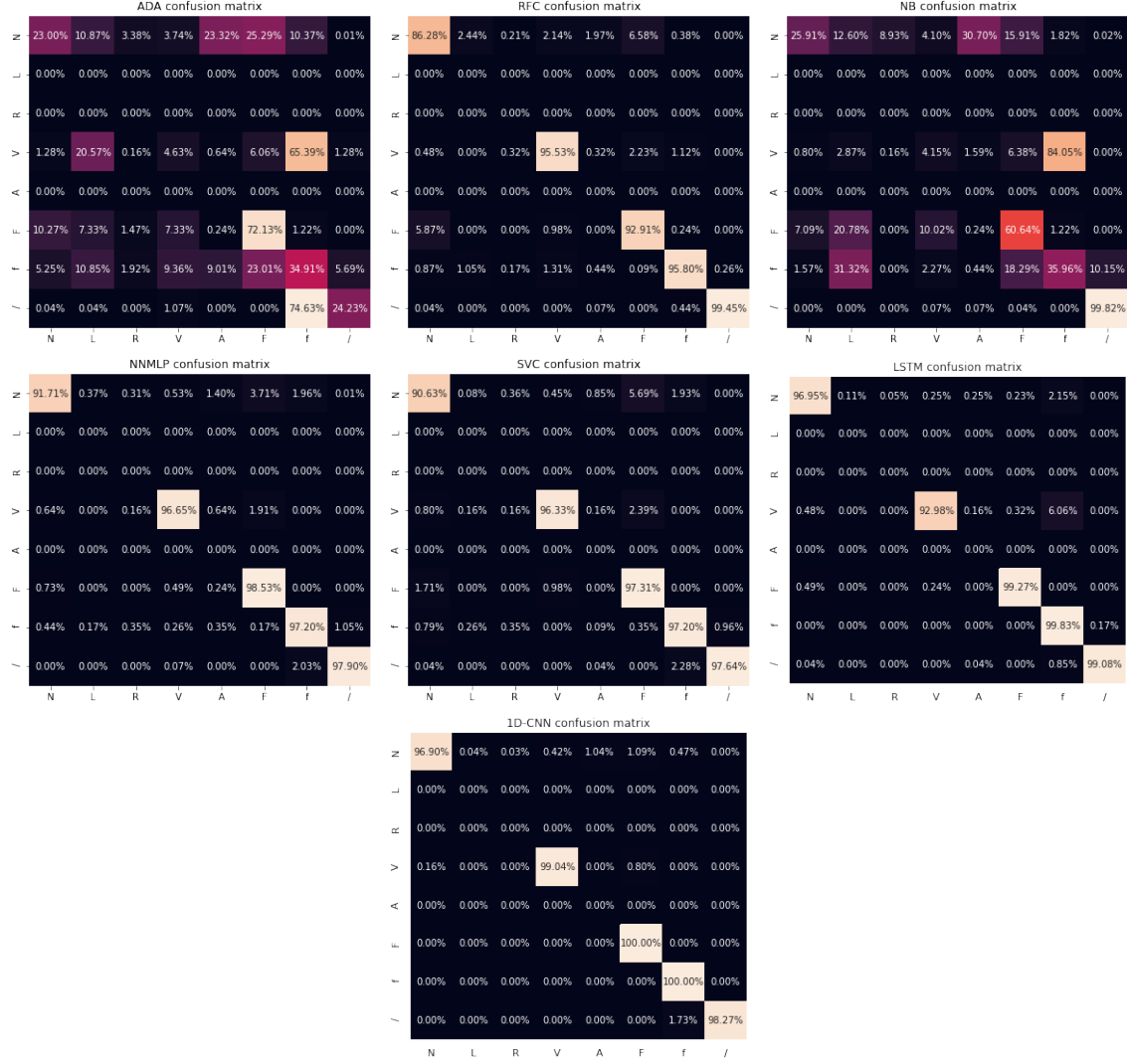


**Figure 25:** Examples of Single Beats of All Classes. (X-Axis: Timestamps, Y-Axis: Voltage) Cross-Validation Confusion Matrices per Model per Class. (X-Axis: Predicted Labels, Y-Axis: True Labels)

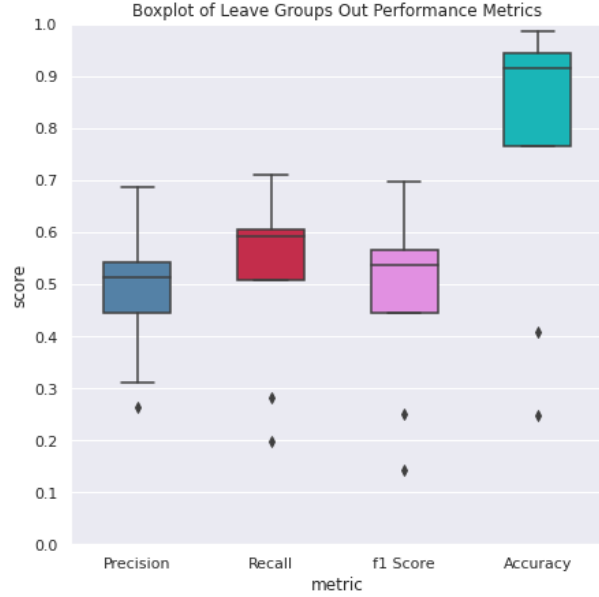
#### 4.2.1 Classification Performance Metrics

Figure 24 shows the macro average performance metric results per class for the patient holdout method. It also shows results for GBC, which was discarded for K-Fold cross-validation. We see that it follows the same trend as before in terms of accuracy, where CNN and LSTM are the best performing models with both of them having accuracy of more than 97%. The precision, recall and f1 score metric give poor results for the patient holdout method where the NNMLP, SVC, CNN, and LSTM scores drop to between 55% and 70%, compared to beats holdout method. The main reason for this is class imbalance since leaving patients out from training dataset is resulting in limited number of beats from one class to be present hence the lower precision and recall. To see scores corrected of this imbalance, the weighted average results can be found on github, where the proportions of the labels of each class are considered.

The low score could also be an issue of unseen data but looking at the confusion matrices in figure 25, it is clear that CNN and LSTM models do not struggle with this issue, giving accuracy of 92% and above for all classes present in the test dataset. It is observed that classes L, R, and A are missing from the test data, which is one of the disadvantages of using Leave Groups Out method. Similarly as before, the diagonals for ADA and NB are irregular indicating bad performance. As for the CNN model which is the best performing model, it obtains 100% accuracy for classifying the F and f class, this is happening due to the unique morphology of fusion of paced beats as they are not completely natural

and are partially created by a pacemaker. This allows us to conclude that the model performs well on unseen data as well.

#### 4.2.2 Quantitative Analysis

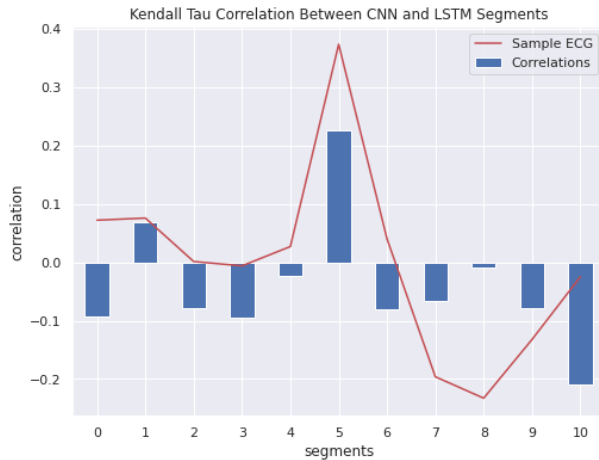


**Figure 26:** All Models Performance Metrics

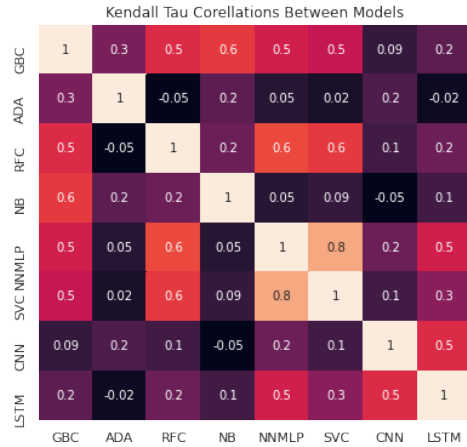
Variable	95% Conf.	Interval
Accuracy	0.543	1.022
Precision	0.369	0.599
Recall	0.372	0.672
f1 Score	0.322	0.632

**Table 5:** Leave Groups Out Statistical Analysis

In the analysis of Leave Groups Out method, tests like Shapiro-Wilk, Kruskal-Wallis H, and Wilcoxon Signed Rank were not implemented since there were no multiple folds to statistically test the data on. However, the rest of the evaluation of the models follow the same pattern as the previous section with the implementation 95% CI on performance metrics and the Kendall tau rank correlation on PFI and Grad-CAM values. Table 5 shows that the CI of precision, recall and f1 score are in the same range, while the CI for accuracy is more spaced out, indicating that the population means of accuracy is in a larger range than the other metrics.



**(a)** Per Segment Correlation between CNN and LSTM Layer Weights



**(b)** Per Model Correlation between Feature Weights

**Figure 27:** Kendall Tau Correlations P-values

Figure 27a shows the Kendall's tau correlation values per segment between the LSTM and CNN layer weights. Here it is observed that segment 5 shows moderate agreement, and segment 10 shows moderate disagreement of correlation, and the rest of the segments are showing no monotonous relation at all. This agreement in the middle of the QRS complex can be visualized in the next figure where the average Grad-CAM values of both CNN and LSTM model are

same at the 5th segment. Figure 27b shows the pairwise Kendall’s tau correlation for the PFI scores between models. PFI values of ADA, NB and CNN have the almost no correlation with other models. This could be due to the bad performance of the ADA and NB models, whereas for CNN model, it could be a result of the feature importance scores favouring completely different segments than the other models. This can be better seen in the next figure which visualizes the PFI values for the CNN model.

We then move on to quantitatively analyse and compare PFI feature importance weights and Grad-CAM correct and mis-classified results per segment. The same L and F classes as the previous section are not compared in this section, as the CNN model predicted the F class with 100% accuracy leaving no incorrect beats to compare, and the patient holdout method did not contain the L class beats. In figure 28 we observe that average CNN and LSTM Grad-CAM values focus on segment 5 of the QRS complex, while the PFI values for both the models lean towards segments 7, 8, 9 i.e. the ST segment. Along with looking at the ST segment, the PFI for CNN model also focuses on the PR interval giving a bump at segment 3. For class V, the CNN model has high Grad-CAM values on the QRS complex, while the LSTM model considers segments 1 and 6 more important. For class /, the CNN model seems to be slightly considering segments 6 and 7 as important, while the LSTM model focuses heavily on segments 5, 6, 7, and 9 i.e., the later part of the QRS complex and ST segment. These inconsistencies that are found in the patient holdout interpretability were not present in the traditional beats holdout method.

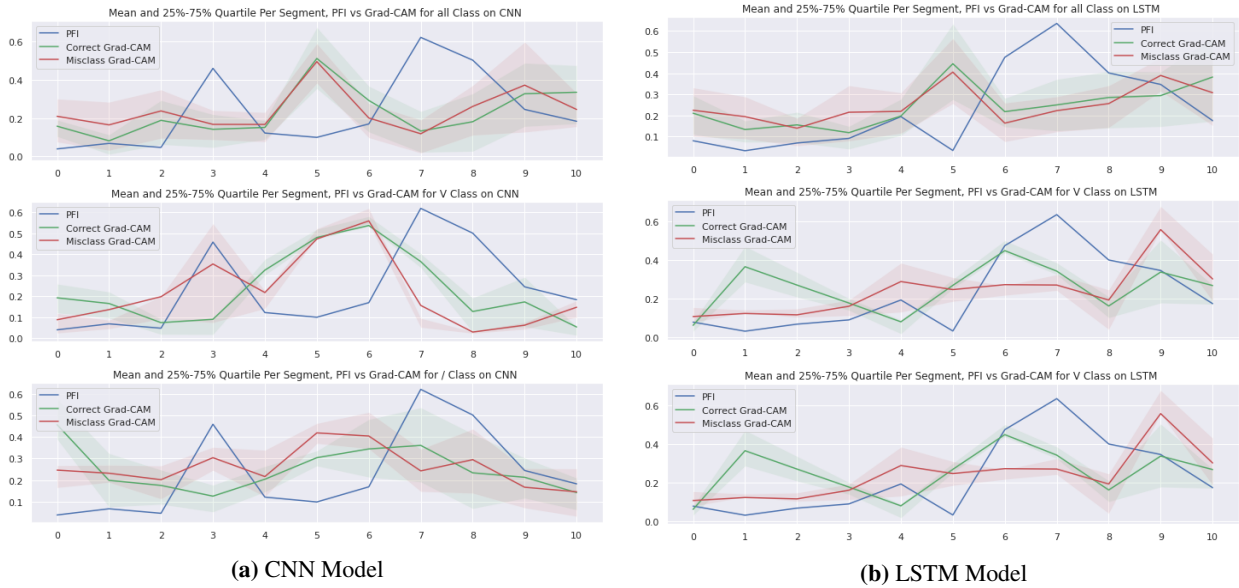


**Figure 28:** Mean and 25%-75% Quartile Values Per Segment - PFI vs Grad-CAM Average (top), V Class (middle), / Class (bottom), for CNN and LSTM Models. (X-Axis: Segments, Y-Axis: Scaled Values)

### 4.3 Variance per Segment

To better understand the Grad-CAM vs PFI comparison plots, variance of segments of the ECG beats per class was plotted as seen in figure 29. We are looking at the variance of each segment to understand where in the signal the classes differ the most, and it would be expected that the segments with the highest variance would be picked up by the ML models, and therefore tells the algorithm most about which class each beat belongs to. It is seen that figure 4.12 has classes L, F, V and / which were previously evaluated in various sections. Class L contains more variance in the ST segment compared to the QRS complex, whereas class F contains variance mostly in the QRS complex. As for /, high variance is observed in the QRS complex, whereas class V shows high variance in both QRS complex and ST segment. The thick blue line shows variance across all beats which has high values concentrated to the middle of the QRS complex. Variance per segment plots for all classes can be found in on github. Taking these variances into account, it is observed that the plots for Grad-CAM comparison per class in figures 23 and 28 show consistency with the model’s predictions on the segments with the most amount of variance.

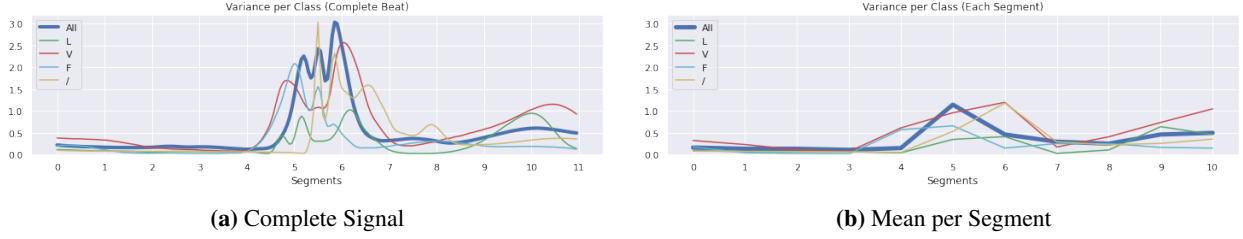


**Figure 29:** Variance per Segment for Classes L, F, f, /, and All Beats. (X-Axis: Segments, Y-Axis: Scaled Values)

## 5 Discussion and Conclusion

### 5.1 Summary

In this study, different interpretability tools to explain ML models for time-series ECG classification problem were investigated. Firstly, the MIT-BIH arrhythmia dataset was split into ECG beats of eight annotation classes, and then ECG classification was performed using eight different classifiers. Next, the ECG beats were divided into 11 segments which would allow us to understand which area of the beats per class were focused on by the models during the prediction making process. K-fold cross-validation (holdout beats) and Leave Groups Out (holdout patients) were the two model evaluation techniques used on the classifiers. Four different interpretability techniques were applied on the models and the resulting explanations were investigated and evaluated using quantitative statistical analysis. The following section will discuss the investigated interpretability techniques before laying down the conclusion and talking about limitations and future work.

### 5.2 Discussion on Interpretability Techniques

One of the biggest disadvantages of PDP is that there is an assumption of independence i.e., it is assumed that features used for computing the partial dependence are not correlated between each other. However, if the features are not correlated, then the PDP display the average influence of the feature in the predictions. The main issue is also that the heterogeneous effects are hidden in PDP as it only displays the marginal effect each class or feature has in the model’s decision-making process. The easy to implement nature of PDP is not advantageous enough to outweigh the issues it faces for time-series interpretability. In this case, the clarity of explanation provided by PDP were uncertain and the metrics were unavailable, which allows us to conclude that this method is not fit for explaining models classifying time-series data.

KernelSHAP is extremely slow which makes it difficult to implement it for many instances. In this case, there are more than 30,000 beats to be tested but only the first 50 instances are used to produce the decision and summary plots for KernelSHAP. For time-series, SHAP has a possibility of hiding biases and intentionally displaying misleading interpretation since it is only designed to deal with 2D data. The only advantage is that with SHAP, global interpretations are consistent with the local explanations. For my investigation, KernelSHAP did provide satisfying explanations which were consistent with both global and local interpretations of the SVC model, which allowed us to look at the overall decision for the dataset along with explaining the behaviour of the model for each class. However, the timing overhead, incompatibility with deep and recurrent neural networks, and the small number of instances explained by this method makes it clear that SHAP is not fit for explaining models classifying time-series data.

Permutation feature importance is the increase in model error when the feature’s information is destroyed, which provides an extremely compressed, global interpretation into the model’s decision-making behaviour. It has a few advantages which include no model retraining, accounting for all interactions between features, and it is comparable across all data types like tabular, text, time-series etc. One of the disadvantages is that it depends on reshuffling features, adding randomness to the data measurements. The model agnostic and global interpretability nature of this method proves to be fairly useful for explaining the model’s behaviour as the results are accurate and consist. However, unlike SHAP there is no local interpretability, which means it is not possible to explain the behaviour of ECG segments for each class of this data.

Grad-CAM created saliency maps which showed each data point’s unique quality per beat which allowed for a very local explanation of the model’s predictive process. These produced coarse localization maps of the important regions allowing us to visualize which segments are more heavily influencing the model’s behaviour. We then approximated global interpretability by averaging the local maps per class. These are implemented on the output of the final 1D-CNN or LSTM layers. This implementation is limited to TensorFlow models making it a model specific interpretability

method. However, having ability to both locally and globally explain deep and recurrent neural network models makes this implementation a very versatile interpretability technique which also allows the users to understand the explanations, unlike PDP. For this reason, Grad-CAM satisfied all the mentioned attributes of interpretability and fidelity of the model’s explanation.

For each explainable interpretability method, it was designated if a attribute is satisfied (S), or if an attribute is unsatisfied (U). All the interpretability methods implemented in this investigation were post-hoc explanations of the model’s decisions, which means the interpretation occurred after the models were finished running. These post-hoc explanations can be seen in the table 6.

To reach a set of pragmatic definitions, interpretability and fidelity were split into general fundamental factors that in conjunction determine the quality of an explanation. This method of qualitative evaluation of interpretability techniques is proposed by Markus et al. [2021]. This leads to the following definitions. Interpretability: An explanation is interpretable if it is unambiguous and yields a single reasoning that is similar for related instances (clarity), the explanation is not too complicated and is presented in a condensed form (parsimony). Interpretability describes the degree to which a user can understand an explanation. Fidelity: An explanation is accurate if the explanation describes the complete dynamic of the given model and provides adequate information to calculate the output for a given input (completeness) and the explanation is correct and is candid to the model’s task (soundness). Fidelity describes the graphic accuracy of the explanation.

**Table 6:** Evaluating Post-hoc Interpretability Methods

Methods	Interpretability				Fidelity	
	Scope	Model	Clarity	Parsimony	Completeness	Soundness
PDP	Global	Specific	U	S	U	U
SHAP	Local	Specific	S	S	U	S
PFI	Global	Agnostic	S	S	U	S
Grad-CAM	Local	Specific	S	S	S	S

### 5.3 Conclusion

The investigation of model interpretability is vital for the application of these models for clinical usage in the healthcare industry. The motivation of this project was to find the best performing interpretability technique to explain various models’ prediction process for time-series ECG classification task.

The results of the ECG classification task showed that the convolutional neural network and the long short-term memory classifiers were the best performing models for both K-Fold cross-validation and Leave Groups Out model evaluation methods. The obtained accuracy for CNN and LSTM models were: 94.1% and 94% for K-Fold cross-validation method, and 98.7% and 97% for Leave Groups Out method. Quantitative hypothesis testing backed the resulting performance metrics in terms of significance levels, which allowed us to conclude that the classification of CNN and LSTM were consistently better than other models. These two neural networks also had the advantage of being interpretable by both Grad-CAM and PFI, which provided both local and global explanations of their prediction process.

In my conclusion of the investigation of interpretability methods, saliency maps using Grad-CAM proved to be the most effective technique to locally interpret neural networks. The advantage of averaging Grad-CAM and neural network layer weights per class and also for the whole dataset, allowed the explanation of the model’s predictions both locally and globally for individual data points, and segments of the ECG beats. The versatile nature of implementing Grad-CAM interpretability on time-series classification made it the most capable technique compared to the rest. PFI had the advantage of being the only model agnostic interpretability technique which explained TensorFlow classifier’s layer weights using a surrogate model, but gave only global explanations of the segments for the entire dataset, and not for each class. Quantitatively comparing PFI and Grad-CAM values allowed for deeper analysis of the difference between local and global explanations. PDP was found to be extremely uninformative at explaining different segments of the ECG beat, while SHAP was too time consuming and explained a very limited amount of data. This allowed me to conclude that PDP and SHAP methods were the worst performing interpretability techniques for ECG data.

Investigating these techniques allowed me to conclude that the proposed neural network and SK-Learn classifiers can be successfully interpreted for time-series ECG classification and are not complete black boxes. The model’s ability to accurately classify the ECG beats by considering the QRS complex more significant than other ECG segments, proved that the prediction process agrees with medical literature i.e., how clinicians and cardiologists classify abnormal ECG beats.

## 5.4 Limitations and Future Work

There is a significant imbalance of classes of ECG beats in the MIT-BIH dataset which makes the model struggle to learn differences between classes even after resampling. The beats are taken from a small number of patients which limits diversity in characteristics of heartbeats. Secondly, most interpretability software and libraries are not created to explain time-series data due to abundance of data points in one signal. These methods explain the model through features of the data and providing 220 data points each for 32,000 beats would not be feasible. Hence, the ECG beats needed to be segmented and given as features to the interpretability software which made it lose significant amount of data points. As for Grad-CAM, one of the limitations is that it struggles to localize multiple occurrences of the same features and may provide false localization of heat-maps with reference to class region. It also gives no explanation of interaction between features and combinations of inputs.

Future work can involve testing larger arrhythmia datasets on better and more fine-tuned deep learning models. Alternative to Grad-CAM attribution method, integrated gradients Sundararajan et al. [2017] could be used to investigate model interpretability on time-series ECG data for more accurate localization of features. The investigation of attention mechanisms Hsu et al. [2019] to recognize critically significant ECG segments associated to model performance could lead to better interpretability, compared to using gradient weights to explain the model’s prediction process.

## References

- Jianhua Wu, Chris P Gale, Marlous Hall, Tatendashe B Dondo, Elizabeth Metcalfe, Ged Oliver, Phil D Batin, Harry Hemingway, Adam Timmis, and Robert M West. Editor’s choice-impact of initial hospital diagnosis on mortality for acute myocardial infarction: A national cohort study. *European Heart Journal: Acute Cardiovascular Care*, 7(2): 139–148, 2018. ISSN 2048-8726.
- George B Moody and Roger G Mark. The impact of the mit-bih arrhythmia database. *IEEE Engineering in Medicine and Biology Magazine*, 20(3):45–50, 2001. ISSN 0739-5175.
- C Molnar. Interpretable machine learning. leanpub. Victoria, 2019.
- Scott M Lundberg and Su-In Lee. A unified approach to interpreting model predictions. *Advances in neural information processing systems*, 30, 2017.
- André Altmann, Laura Tološi, Oliver Sander, and Thomas Lengauer. Permutation importance: a corrected feature importance measure. *Bioinformatics*, 26(10):1340–1347, 2010. ISSN 1460-2059.
- Ramprasaath R Selvaraju, Michael Cogswell, Abhishek Das, Ramakrishna Vedantam, Devi Parikh, and Dhruv Batra. Grad-cam: Visual explanations from deep networks via gradient-based localization. In *Proceedings of the IEEE international conference on computer vision*, pages 618–626, 2017.
- Aswathy Velayudhan and Soniya Peter. Noise analysis and different denoising techniques of ecg signal-a survey. *IOSR journal of electronics and communication engineering*, 1(1):40–44, 2016.
- Christopher J Kelly, Alan Karthikesalingam, Mustafa Suleyman, Greg Corrado, and Dominic King. Key challenges for delivering clinical impact with artificial intelligence. *BMC medicine*, 17(1):1–9, 2019. ISSN 1741-7015.
- Mohammad Kachuee, Shayan Fazeli, and Majid Sarrafzadeh. Ecg heartbeat classification: A deep transferable representation. In *2018 IEEE international conference on healthcare informatics (ICHI)*, pages 443–444. IEEE, 2018. ISBN 153865377X.
- U Rajendra Acharya, Hamido Fujita, Oh Shu Lih, Yuki Hagiwara, Jen Hong Tan, and Muhammad Adam. Automated detection of arrhythmias using different intervals of tachycardia ecg segments with convolutional neural network. *Information sciences*, 405:81–90, 2017. ISSN 0020-0255.
- Saroj Kumar Pandey and Rekh Ram Janghel. Automatic detection of arrhythmia from imbalanced ecg database using cnn model with smote. *Australasian physical and engineering sciences in medicine*, 42(4):1129–1139, 2019. ISSN 1879-5447.
- Junli Gao, Hongpo Zhang, Peng Lu, and Zongmin Wang. An effective lstm recurrent network to detect arrhythmia on imbalanced ecg dataset. *Journal of healthcare engineering*, 2019, 2019. ISSN 2040-2295.
- Sajad Mousavi and Fatemeh Afghah. Inter-and intra-patient ecg heartbeat classification for arrhythmia detection: a sequence to sequence deep learning approach. In *ICASSP 2019-2019 IEEE International Conference on Acoustics, Speech and Signal Processing (ICASSP)*, pages 1308–1312. IEEE, 2019. ISBN 1479981311.
- G Stiglic, P Kocbek, N Fijacko, M Zitnik, K Verbert, and L Cilar. Interpretability of machine learning based prediction models in healthcare. arxiv 2020. *arXiv preprint arXiv:2002.08596*, 2019.

- Sricharan Vijayarangan, Balamurali Murugesan, R Vignesh, SP Preejith, Jayaraj Joseph, and Mohansankar Sivaprakasam. Interpreting deep neural networks for single-lead ecg arrhythmia classification. In *2020 42nd Annual International Conference of the IEEE Engineering in Medicine and Biology Society (EMBC)*, pages 300–303. IEEE, 2020. ISBN 1728119901.
- Yola Jones, Fani Deligianni, and Jeff Dalton. Improving ecg classification interpretability using saliency maps. In *2020 IEEE 20th International Conference on Bioinformatics and Bioengineering (BIBE)*, pages 675–682. IEEE, 2020. ISBN 1728195748.
- Fabian Pedregosa, Gaël Varoquaux, Alexandre Gramfort, Vincent Michel, Bertrand Thirion, Olivier Grisel, Mathieu Blondel, Peter Prettenhofer, Ron Weiss, and Vincent Dubourg. Scikit-learn: Machine learning in python. *the Journal of machine Learning research*, 12:2825–2830, 2011. ISSN 1532-4435.
- Ian Jolliffe. Principal component analysis (pp. 1094-1096). *Springer Berlin Heidelberg. RESUME SELİN DEĞİRMECİ Marmara University, Goztepe Campus ProQuest Number: ProQuest*. Copyright of the Dissertation is held by the Author. All Rights Reserved, 28243034:28243034, 2011.
- Laurens Van der Maaten and Geoffrey Hinton. Visualizing data using t-sne. *Journal of machine learning research*, 9 (11), 2008. ISSN 1532-4435.
- Leland McInnes, John Healy, and James Melville. Umap: Uniform manifold approximation and projection for dimension reduction. *arXiv preprint arXiv:1802.03426*, 2018.
- Rahul Kher. Signal processing techniques for removing noise from ecg signals. *J. Biomed. Eng. Res*, 3(101):1–9, 2019.
- Jacinto Carrasco, Salvador García, MM Rueda, Swagatam Das, and Francisco Herrera. Recent trends in the use of statistical tests for comparing swarm and evolutionary computing algorithms: Practical guidelines and a critical review. *Swarm and Evolutionary Computation*, 54:100665, 2020. ISSN 2210-6502.
- Janez Demšar. Statistical comparisons of classifiers over multiple data sets. *The Journal of Machine Learning Research*, 7:1–30, 2006. ISSN 1532-4435.
- Pauli Virtanen, Ralf Gommers, Travis E Oliphant, Matt Haberland, Tyler Reddy, David Cournapeau, Evgeni Burovski, Pearu Peterson, Warren Weckesser, and Jonathan Bright. Scipy 1.0: fundamental algorithms for scientific computing in python. *Nature methods*, 17(3):261–272, 2020. ISSN 1548-7105.
- William R Knight. A computer method for calculating kendall’s tau with ungrouped data. *Journal of the American Statistical Association*, 61(314):436–439, 1966. ISSN 0162-1459.
- Aniek F Markus, Jan A Kors, and Peter R Rijnbeek. The role of explainability in creating trustworthy artificial intelligence for health care: a comprehensive survey of the terminology, design choices, and evaluation strategies. *Journal of Biomedical Informatics*, 113:103655, 2021. ISSN 1532-0464.
- Mukund Sundararajan, Ankur Taly, and Qiqi Yan. Axiomatic attribution for deep networks. In *International conference on machine learning*, pages 3319–3328. PMLR, 2017. ISBN 2640-3498.
- En-Yu Hsu, Chien-Liang Liu, and Vincent S Tseng. Multivariate time series early classification with interpretability using deep learning and attention mechanism. In *Pacific-Asia Conference on Knowledge Discovery and Data Mining*, pages 541–553. Springer, 2019.